Koc. J. Sci. Eng., 7(2): (2024) 151-157 https://doi.org/10.34088/kojose.1391406

Kocaeli University

Kocaeli Journal of Science and Engineering

http://dergipark.org.tr/kojose

Investigation of the Post-Processing Heat Treatments on Hot Tensile Properties of Selectively Laser Melted IN939 Superalloy

Fatih GULER [1], Aylin S. KAHRAMAN [2], Burak HORASAN [3], Guney Mert BILGIN [4], Ozgul KELES [5,*], Huseyin AYDIN [6,*]

[1] *Metallic and Structural Materials Technologies Research Group, TUBITAK MAM, Kocaeli, Turkey,* ***ORCID:*** *0000-0002-3647-6487*
[2] *Metallic and Structural Materials Technologies Research Group, TUBITAK MAM, Kocaeli, Turkey,* ***ORCID:*** *0000-0002-6465-5415*
[3] *Department of Materials Science and Engineering, Gebze Technical University, Kocaeli, Turkey,* ***ORCID:*** *0000-0002-4527-5783*
[4] *TUSAS Engine Industries, Inc. (TEI), Eskisehir, Turkey,* ***ORCID:*** *0000-0002-8909-0633*
[5] *Department of Metallurgical and Materials Engineering, Istanbul Technical University, Maslak, İstanbul, Turkey,* ***ORCID:*** *0000-0002-4656-5563*
[6] *Metallic and Structural Materials Technologies Research Group, TUBITAK MAM, Kocaeli, Turkey,* ***ORCID:*** *0000-0002-8600-2984*

Article Info

Research paper

Received : *November 15, 2023*
Accepted : *April 27, 2024*

Keywords

Additive Manufacturing
Hot Isostatic Pressing (HIP)
Hot Tensile Testing
Inconel 939 (IN939)
Selective Laser Melting (SLM)
Vacuum Heat Treatment

Abstract

In recent years, the Selective Laser Melting (SLM) process has become the focus of research due to its wide range of benefits and easy fabrication advantageous in the mass production of nickel-based superalloys. However, the mechanical properties of additively manufactured nickel-based superalloys are insufficient for service conditions. Therefore, heat treatment studies are necessary to achieve desired microstructures for better mechanical properties. In this concept, it is aimed to replace melt pool boundaries and to obtain more equiaxed fine grain boundaries via heat treatment studies. This study deals with the effect of post-heat treatment studies on the microstructure and mechanical properties of selectively laser-melted Inconel 939 (IN939) superalloy. As-built and heat-treated (HIP&VHT) samples were characterized via optical and electron microscopy techniques. Transition temperatures and phases were analyzed using XRD, DSC, and Thermo-Calc simulation techniques. Finally, the effect of the hot tensile test on γ′ formation and morphology in the microstructure was investigated. Overall, the study tried to provide insight into whether the post-processes are necessary for modifying microstructure and achieving optimal mechanical properties. It was observed that both HIP and VHT had a beneficial impact on the elongation in comparison to the as-built conditions. However, no noticeable differences were achieved in ultimate tensile and yield stress.

1. Introduction

Nickel-based superalloys are highly valued in the aviation and energy industries for their exceptional resistance to oxidation and ability to withstand high temperatures. However, traditional manufacturing methods have limitations that hinder efficiency, such as high costs and lengthy production times [1–4]. To address these issues, researchers have explored new manufacturing processes such as selective laser melting (SLM) for nickel-based superalloys, which offer expanded design possibilities and reduced time and costs [5–9].

SLM is a 3D printing technique that utilizes a high power-density laser to melt and fuse metallic powders. While SLM has many advantages over conventional methods, manufacturing nickel-based superalloys with this technique can present certain challenges. Microstructural heterogeneity results from methods used in building parts inevitably lead to mechanical heterogeneity [10-12]. Consequently, post-processes like hot isostatic pressing (HIP) and vacuum heat treatments (VHT) are necessary to achieve the desired microstructure [2, 13].

IN939 is a superalloy primarily composed of nickel and boasts an FCC crystal structure matrix. It is highly resistant to corrosion and oxidation at temperatures as high as 850°C, making it an ideal material for environments that require such properties [14]. However, the mechanical properties of the alloy can vary depending on its processing history, due to its precipitation-hardening nature. Exposure to high temperatures can change the properties, as the γ’ becomes coarser and other thermodynamically stable phases form in the

* Corresponding Author: ozgulkeles@itu.edu.tr, aydin.huseyin@tubitak.gov.tr

This article is orally presented as a proceeding at the 3rd International Symposium on Characterization, held in Istanbul between September 6-8, 2023.

microstructure [9], [15], [16].

The tensile properties of alloys are important mechanical performance indicators for the structural design of key engine components. Therefore, the tensile properties of Inconel 939 alloy, manufactured by different production processes and heat treatments have been studied in the literature [17–21]. Modifying the alloy composition, aging temperature and time can lead to improved tensile properties by altering the precipitation amounts of phases. However, there is still a lack of literature on how to effectively utilize post-processes to transform particle boundary to grain boundary in additive manufacturing and achieve comparable and desirable mechanical properties [11, 16, 22, 23].

This study presents an examination of the effects of post-heat treatments, namely HIP and VHT, on Inconel 939 superalloys produced through additive manufacturing, and evaluates the formation of γ and γ′ morphology after being exposed to hot tensile test conditions.

2. Materials and Methods

Gas-atomized Inconel 939 powder supplied by EOS GmbH (Nickel Alloy IN939) was used for the SLM process. Table 1 shows the nominal chemical composition measured by the ICP-combustion method.

Table 1. Nominal chemical composition of the IN939 powder (in wt%).

Cr	***Co***	***Al***	***Ti***	***Ta***	***Ni***
22.5	19.3	1.9	3.7	1.4	
Nb	***W***	***Zr***	***B***	***C***	balance
1.0	2.0	0.1	<0.01	0.15	

The Mastersizer 2000 (Malvern Instruments Ltd, UK) system was employed to measure the particle size distribution of the powder following ISO 13320-1 standard. To ensure accuracy, a small amount of each IN939 powder sample, featuring a refractive index of 1.520, was mixed with deionized water with a refractive index of 1.330. The powders were then subjected to mechanical and ultrasonic stirring, circulation, and degassing before measurement. The resulting average d50 and d90 were found to be 34.288 µm and 60.877 µm, respectively (see Figure 1).

The morphology of IN939 powder was investigated using a HITACHI SU7000 scanning electron microscope (SEM). The powder particles exhibited a diverse range of shapes and sizes, with some displaying a spherical morphology and formations that resemble satellites (Figure 2).

An EOS M 290 metal 3D printer using the SLM technique, equipped with a 400W yttrium fiber laser was used to fabricate cylindrical bar specimens from IN939 powder (Figure 3). Process parameter sets for IN939 alloy supplied by EOS company were used to produce the specimens [24]. To analyze the microstructure of the specimens, optical and scanning electron microscopy (SEM) techniques were utilized. The Olympus BX53M inverted microscope was used for optical microscopy, while electron microscopy was conducted on a HITACHI SU7000 that was equipped with an Energy-Dispersive X-ray Spectroscopy (EDX) detector.

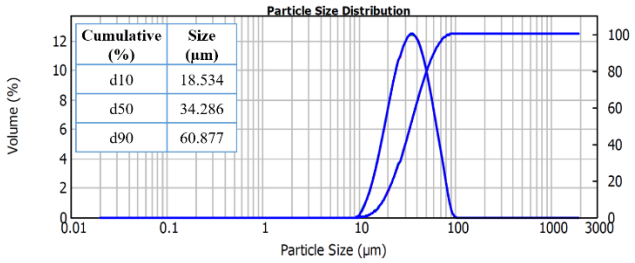

Figure 1. Particle size distribution of the IN939 powder.

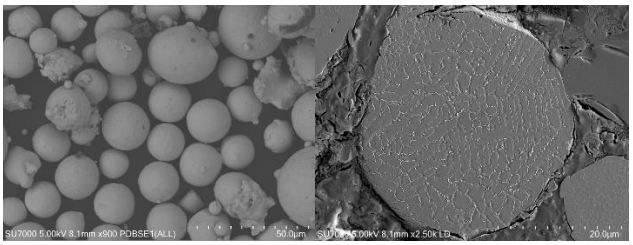

Figure 2. SEM images of IN939 superalloy powder.

Figure 4 displays micrographs that depict the as-built state of SLM-processed samples. The arch-shaped molten pool boundaries resulting from the layer-by-layer processing are visible in Figure 4a. On further examination, Figure 4b highlights the dendritic and interdendritic structure, revealing the significant impact of heat flux on the microstructure of SLM material during layer-wise manufacturing. As a result, anisotropic microstructural features are prominently displayed [25].

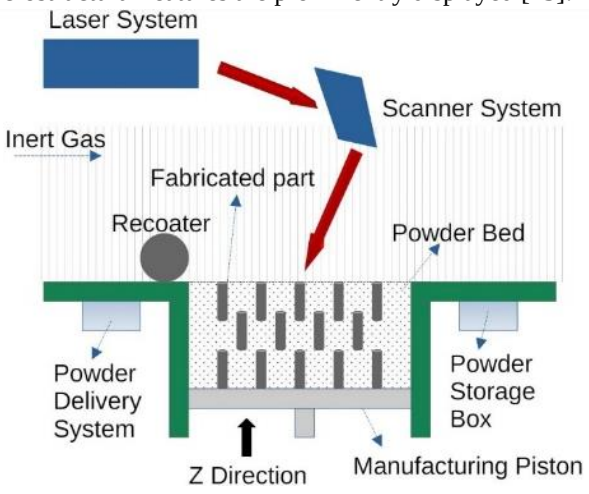

Figure 3. Schematic diagram of the SLM system used in this study.

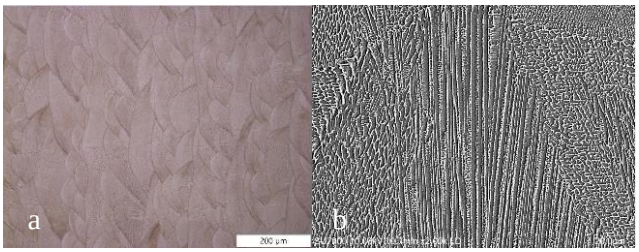

Figure 4. Micrographs for the as-built condition: (a) optical microscope and (b) scanning electron microscope.

The post-heat treatment parameters were determined through a combination of Differential scanning calorimetry (DSC) and Thermo-Calc simulation techniques. DSC analysis was conducted using the Seteram Setsys Evolution in an argon atmosphere with a flow rate of 20 mL.min^{-1}, recording the heat flux during heating and cooling of the samples at a rate of 10°C min^{-1} from room temperature to 1450°C. For modeling studies, the Thermo-Calc program was used with the TCNI10 Nickel-based Superalloys Database. The temperature-dependent properties of the samples were matched with DSC and microstructure analyses using the program [25].

To investigate the impact of heat treatment on the as-built samples, two distinct methods were utilized. The first, HT1, entailed high temperature and pressure solutionizing using the Quintus QIH-21 hot isostatic press (HIP), followed by a two-stage aging process. The second, HT2, involved solutionizing without pressure and two-stage aging in a TAV brand vacuum heat treatment furnace. The Time-Temperature diagram for the heat treatments is given in Figure 5.

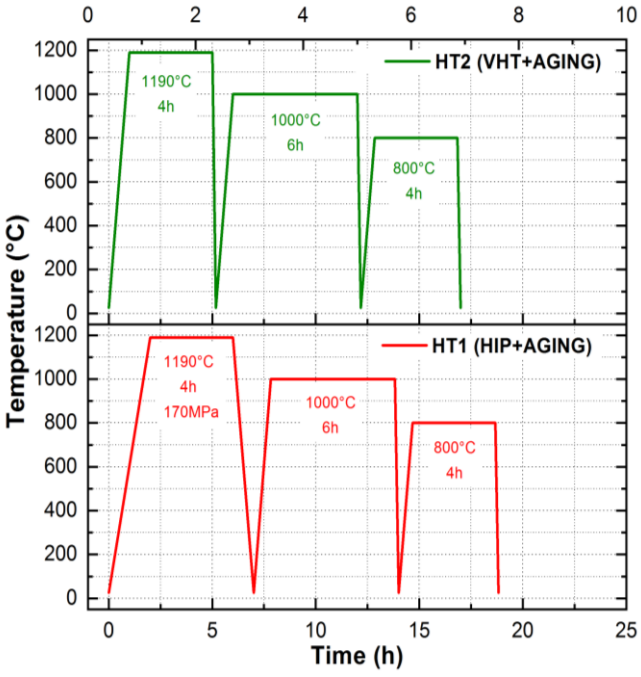

Figure 5. Time-Temperature diagram for the heat treatments.

To determine the crystalline phases, Rigaku SmartLab was used for X-ray diffraction (XRD) analysis with CuKα radiation at a 9 kW anode X-ray source.

The cylindrical bar samples were machined into dog bone shapes according to ASTM E8 and ASTM E21 standards. Hot tensile tests were conducted at 750°C using a Zwick Z600 model universal testing machine with a preload of 400N, at a speed of 0.00007 1/s up to the yield point and 0.0014 1/s after the yield point.

3. Results and Discussion

Figure 6 shows the temperature-dependent phase analysis of the alloy. According to the solidification curves, the liquid phase is in complete equilibrium from 1400ºC to 1356ºC. The γ phase begins to form at 1356ºC, starting the solidification. Between 1264ºC to 1091ºC, a γ matrix is formed, which is almost entirely dissolved, except for small amounts of metal carbide (MC) phase. The liquidus temperature is 1356ºC, the solidus temperature is 1264ºC, and the solvus temperature is 1091ºC.

In Figure 7a, it is observed that the as-built sample shows a significant change in heat flow between ~1080°C and ~1107°C, which can attributed to the dissolution of γ' into the γ matrix. The carbide melting and dissolution were shown as two separate peaks. This indicates that carbide dissolution occurs around ~1320°C, while the matrix melting continues up to ~1358°C. On the other hand, the cooling provided a clearer temperature range for the precipitation of the MC-type carbides, which was between 1326°C-1340°C (Figure 7b) [26].

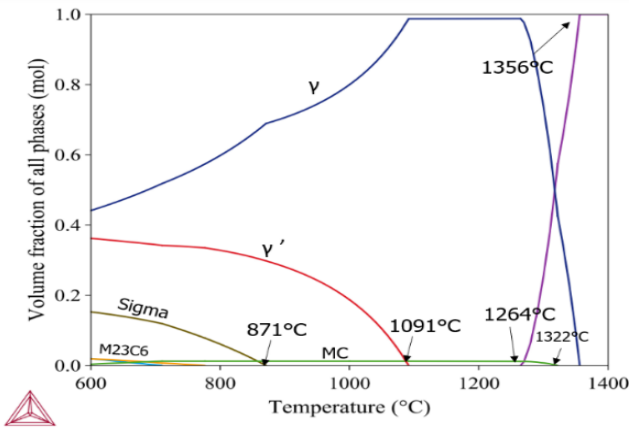

Figure 6. Temperature-dependent phase analysis of IN939 via Thermo-Calc software.

The XRD profiles for the heat-treated and as-built samples were compared in Figure 8. The XRD spectra for all samples showed face-centered cubic (FCC) peaks linked to the γ and/or γ' phases. The diffraction peaks indicated the diffraction of (111), (200), (202), (311), and

(222) planes of the γ solid solution and/or γ' precipitates. No unforeseen phases were identified in any sample during the analysis.

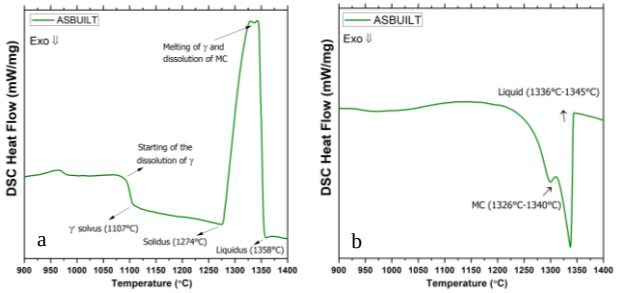

Figure 7. DSC graphs for heating (a) and cooling (b) runs.

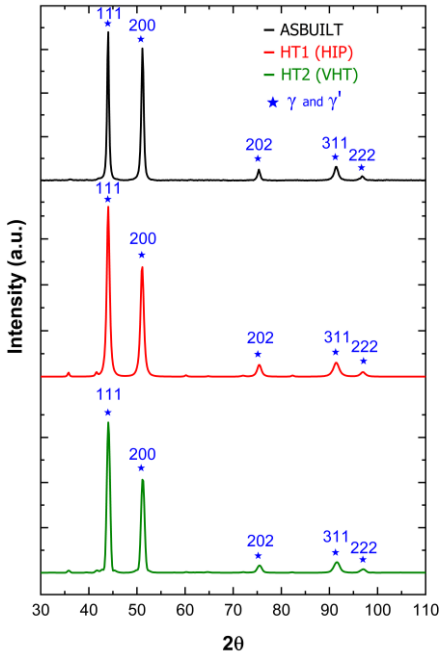

Figure 8. XRD analysis of as-built and heat-treated samples.

SEM microstructures (Figure 9 and Figure 10) revealed that the melt-pools that were present in the as-built specimens were not observed in any of the samples after heat treatments. It was observed that the microstructure of each heat-treated sample was almost completely uniform, with fine grains that maintained their columnar structure and aligned in the building direction due to the fast solidification process of melt-pool structure during the joining process. Further analysis revealed the formation of spherical gamma prime precipitates, as well as the larger carbides that were Ti and Ta rich and present at the grain boundaries and intergranular areas. It is worth noting that no plate-like phases were observed in the microstructures upon investigation [15].

Figure 11 displays the results of the hot tensile test conducted on the as-built and heat-treated samples at 750°C. The results demonstrate that both HT1 and HT2 have led to a rise in % elongation in comparison to the as-built state. Nonetheless, there were no significant differences in UTS and yield stress between the two heat treatment procedures.

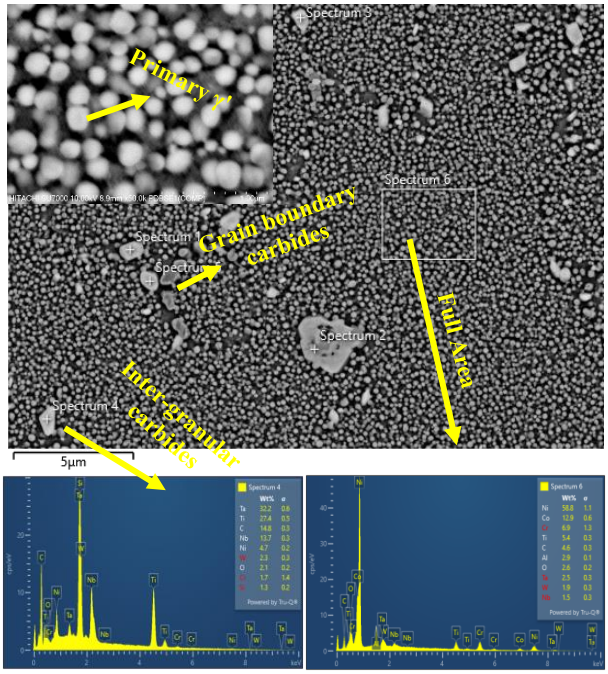

Figure 9. SEM images of HT1 (HIP) condition samples.

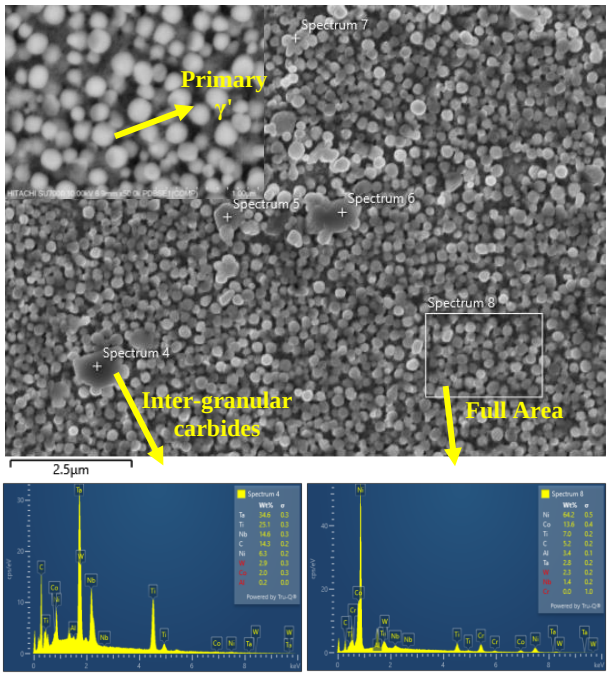

Figure 10. SEM images of HT2 (VHT) condition samples.

In Figure 12, it appears that there were changes in the microstructure near the fractured surface. As illustrated in Figure 12a, the cross-section of the fracture areas was encapsulated in bakelite cylinders. During the hot tensile test, the γ' precipitate in HT1 underwent directional

coarsening or distortion, transforming from a spherical to a plate-like shape, as illustrated in Figure 12b. In contrast to HT1 condition, HT2 exhibited gamma prime coalescence, which was distributed across the different areas of microstructure.

Table 2 revealed an unexpected observation: despite having different γ' volume ratios (%) due to aging conditions, both HT1 and HT2 samples fractured at similar γ' volume ratios during tensile testing. It is known that increasing tensile temperature increases the γ volume ratio due to coarsening and decreases γ' volume ratio due to raftening and anti-phase boundary. Therefore, it can be deduced that dislocation mobility on the coarse γ matrix may be the underlying cause of this failure mechanism.

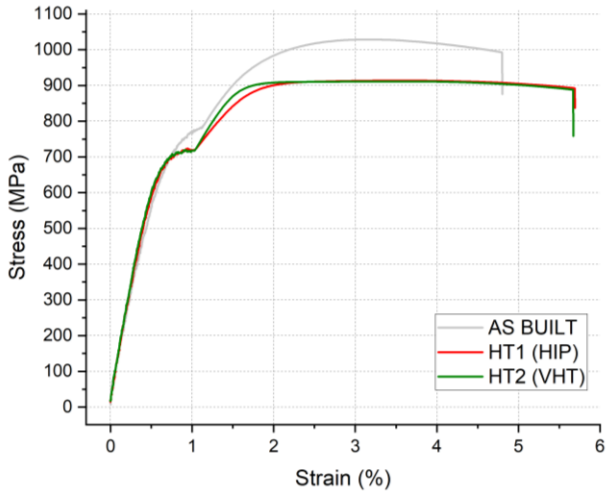

Figure 11. Stress (MPa) – Strain (%) curves of SLM-processed IN939 samples at 750°C.

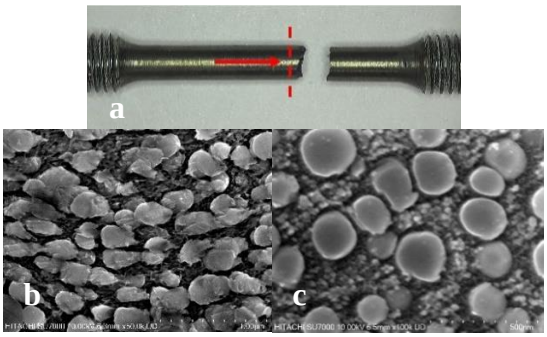

Figure 12. Encapsulation of the cross-section of fracture area (a). Microstructure of HT1 (b) and HT2 (c) samples after hot tensile tests.

Table 2. γ and γ' ratios (%) after hot tensile tests.

Sample	Heat Treated Samples (%)		After Hot Tensile Tests (%)	
	γ	γ'	γ	γ'
HT1 (HIP)	55.2	44.8	68.4	31.6
HT2 (VHT)	45.1	54.9	67.9	32.1

4. Conclusion and Future Studies

This research aimed to investigate the effects of post-heat treatments on the microstructure and hot tensile properties of an additively manufactured IN939. It was observed that γ' in both HT1 and HT2 showed slight morphology change, but no recrystallization was observed.

It is clear that the heat treatment had a positive impact on elongation in hot tensile tests when compared to the as-built condition. However, there was no significant difference in ultimate tensile and yield stress values in comparison to the two heat treatment procedures.

Another important observation was that even though HT1 and HT2 conditions have different γ' volume ratios (%), both heat-treated samples fractured at very similar γ' volume ratios (%) after tensile tests. This suggests a possible failure mechanism due to dislocation mobility on coarse γ matrix rather than γ' rafting mechanism.

To gain a better understanding of the alloy's performance under service conditions, future studies may involve the utilization of newly modified recipes, advanced microstructural characterization, and conducting additional mechanical tests such as creep rupture tests.

Declaration of Ethical Standards

The authors of this article declare that the materials and methods used in this study do not require ethical committee permission and/or legal-special permission.

Conflict of Interest

The authors declare that they have no known competing financial interests or personal relationships that could have appeared to influence the work reported in this paper.

Acknowledgments

TUBITAK TEYDEB supported the study with project code 3219504. The authors would like to express their gratitude to the Metallic Materials Technologies Research Group at TUBITAK Marmara Research Center for their assistance with experimental support, as well as to TUSAS-TEI for their in-kind contribution.

References

[1] M. M. Kirka and P. Fernandez-Zelaia, “Additive Materials for High Temperature Applications,” in Encyclopedia of Materials: Metals and Alloys, F. G. Caballero, Ed., Oxford: Elsevier, 2022, pp. 529–536. doi: https://doi.org/10.1016/B978-0-12-

819726-4.00110-1

[2] A. Mostafaei *et al.*, "Additive manufacturing of nickel-based superalloys: A state-of-the-art review on process-structure-defect-property relationship," *Prog. Mater. Sci.*, vol. 136, p. 101108, 2023, doi: https://doi.org/10.1016/j.pmatsci.2023.101108.

[3] W. Song *et al.*, "A new approach to design advanced superalloys for additive manufacturing," *Addit. Manuf.*, vol. 84, p. 104098, 2024, doi: https://doi.org/10.1016/j.addma.2024.104098.

[4] B. Wahlmann, M. Markl, and C. Körner, "A thermo-mechanical model for hot cracking susceptibility in electron beam powder bed fusion of Ni-base superalloys," *Mater. Des.*, vol. 237, p. 112528, 2024, doi: https://doi.org/10.1016/j.matdes.2023.112528.

[5] N. J. Harrison, "Selective Laser Melting of Nickel Superalloys : solidification , microstructure and material response," 2016.

[6] P. Kanagarajah, F. Brenne, T. Niendorf, and H. J. Maier, "Inconel 939 processed by selective laser melting: Effect of microstructure and temperature on the mechanical properties under static and cyclic loading," 2013. doi: 10.1016/j.msea.2013.09.025.

[7] Randy Bowman, "Superalloys: A Primer and History," in Superalloys: A Primer and History, [Online]. Available: https://www.tms.org/meetings/specialty/superalloys2000/superalloyshistory.html

[8] M. Doi, D. Miki, T. Moritani, and T. Kozakai, "Gamma/gamma-prime microstructure formed by phase separation of gamma-prime precipitates in a Ni-Al-Ti alloy," in *Proceedings of the International Symposium on Superalloys*, 2004. doi: 10.7449/2004/superalloys_2004_109_114.

[9] W. Philpott, M. A. E. Jepson, and R. C. Thomson, "Comparison of the effects of a conventional heat treatment between cast and selective laser melted IN939 alloy," 2016.

[10] M. N. Doğu et al., "Effect of solution heat treatment on the microstructure and crystallographic texture of IN939 fabricated by powder bed fusion-laser beam," J. Mater. Res. Technol., vol. 24, pp. 8909–8923, 2023, doi: https://doi.org/10.1016/j.jmrt.2023.0

[11] A. Mashhuriazar, C. Hakan Gur, Z. Sajuri, and H. Omidvar, "Effects of heat input on metallurgical behavior in HAZ of multi-pass and multi-layer welded IN-939 superalloy," J. Mater. Res. Technol., vol. 15, pp. 1590–1603, 2021, doi: https://doi.org/10.1016/j.jmrt.2021.08.113

[12] S. Sui, C. Zhong, J. Chen, A. Gasser, W. Huang, and J. H. Schleifenbaum, "Influence of solution heat treatment on microstructure and tensile properties of Inconel 718 formed by high-deposition-rate laser metal deposition," J. Alloys Compd., vol. 740, pp. 3

[13] J. Risse, "Additive Manufacturing of Nickel-Base Superalloy IN738LC by Laser Powder Bed Fusion," 2019.

[14] S. A. Raza, O. E. Canyurt, and H. K. Sezer, "A systematic review of Inconel 939 alloy parts development via additive manufacturing process," *Heliyon*, vol. 10, no. 3, p. e25506, 2024, doi: https://doi.org/10.1016/j.heliyon.2024.e25506.

[15] S. Banoth, C. W. Li, Y. Hiratsuka, and K. Kakehi, "The effect of recrystallization on creep properties of alloy in939 fabricated by selective laser melting process," 2020. doi: 10.3390/met10081016.

[16] G. Sjöberg *et al.*, "Evaluation of the IN 939 alloy for large aircraft engine structures," in *Proceedings of the International Symposium on Superalloys*, 2004. doi: 10.7449/2004/superalloys_2004_441_450.

[17] A. S. Shaikh, M. Rashidi, K. Minet-Lallemand, and E. Hryha, "On as-built microstructure and necessity of solution treatment in additively manufactured Inconel 939," *Powder Metall.*, vol. 66, no. 1, pp. 3–11, 2023, doi: 10.1080/00325899.2022.2041787.

[18] T. Zou et al., "Effect of temperature on tensile behavior, fracture morphology, and deformation mechanisms of Nickel-based additive manufacturing 939 superalloy," J. Alloys Compd., vol. 959, p. 170559, 2023, doi: https://doi.org/10.1016/j.jallcom.2023.1705

[19] I. Šulák, T. Babinský, A. Chlupová, A. Milovanović, and L. Náhlík, "Effect of building direction and heat treatment on mechanical properties of Inconel 939 prepared by additive manufacturing," *J. Mech. Sci. Technol.*, vol. 37, no. 3, pp. 1071–1076, 2023, doi: 10.1007/s12206-022-2101-7.

[20] D. Deng, "Additively Manufactured Inconel 718 : Microstructures and Mechanical Properties," 2018.

[21] B. Zhang, H. Ding, A. C. Meng, S. Nemati, S. Guo, and W. J. Meng, "Crack reduction in Inconel 939 with Si addition processed by laser powder bed fusion additive manufacturing," Addit.

Manuf., vol. 72, p. 103623, 2023, doi: https://doi.org/10.1016/j.addma.2023.103623.

[22] D. Deng, R. L. Peng, H. Brodin, and J. Moverare, "Microstructure and mechanical properties of Inconel 718 produced by selective laser melting: Sample orientation dependence and effects of post heat treatments," *Mater. Sci. Eng. A*, 2018, doi: 10.1016/j.msea.2017.12.043.

[23] J. Xu, H. Gruber, D. Deng, R. L. Peng, and J. J. Moverare, "Short-term creep behavior of an additive manufactured non-weldable Nickel-base superalloy evaluated by slow strain rate testing," *Acta Mater.*, vol. 179, pp. 142–157, 2019, doi: 10.1016/j.actamat.2019.08.034.

[24] R. Gusain, M. Dodaran, P. Gradl, N. Shamsaei, and S. Shao, "The Influence of Heat Treatments on the Microstructure and Tensile Properties of Additively Manufactured Inconel 939," 2023.

[25] A. Formenti, A. Eliasson, A. Mitchell, and H. Fredriksson, "Solidification sequence and carbide precipitation in Ni-base superalloys IN718, IN625 AND IN939," *High Temp. Mater. Process.*, vol. 24, Jun. 2005, doi: 10.1515/HTMP.2005.24.4.239.

[26] M. Jahangiri, "Study on incipient melting in cast Ni base IN939 superalloy during solution annealing and its effect on hot workability," *Mater. Sci. Technol.*, vol. 28, pp. 1402–1413, Jun. 2012.